Supplementary Materials:

A high-capacity dual-electrolyte aluminum/air electrochemical cell

Lei Wang,[a] Fude Liu,[a] Wentao Wang,[a] Guandong Yang,[a] Zhuangchun Wu[b] and Michael K.H. Leung[c]*

[a]Department of Mechanical Engineering, The University of Hong Kong, Hong Kong, China

[b]School of Materials Science and Engineering, Nanjing University of Science and Technology, Nanjing 210094, China

[c]Ability R&D Energy Research Centre, School of Energy and Environment, City University of Hong Kong, Hong Kong, China

*Corresponding author: Fude Liu; Electronic mail: fordliu@hku.hk; Department of Mechanical Engineering, The University of Hong Kong, Pokfulam Road, Hong Kong; phone: (+852) 2859 2631; FAX: (+852) 2858-5415

1. Characteristics of typical metal/air cells

Table S1 Characteristics of typical metal/air cells with theoretical values*

Metal anode	Electrochemistry†	Gravimetric capacity§ (mAh g^{-1})	Volumetric capacity§ (mAh cm^{-3})	Cell voltage (V)	Gravimetric energy density§ (Wh kg^{-1})	Volumetric energy density§ (Wh L^{-1})
Li	Anode: $Li \leftrightarrow Li^+ + e^-$ Cathode: (I) $2Li^+ + O_2 + 2e^- \leftrightarrow Li_2O_2$ (aprotic) $(II)\ O_2 + 4H^+ + 4e^- \leftrightarrow 2H_2O\ (acidic)$ $(III) O_2 + 2H_2O + 4e^- \leftrightarrow 4OH^-\ (alkaline)$	3861	2062	(I) 2.96 (ref. 1) (II) 4.26 (ref. 2) (III) 3.43 (ref. 2)	(I) 11429 (II) 16448 (III) 13243	(I) 6104 (II) 8784 (III) 7073
Na	Anode: $Na \leftrightarrow Na^+ + e^-$ Cathode: (III) $O_2 + 2H_2O + 4e^- \leftrightarrow 4OH^-\ (alkaline)$ (IV) $Na^+ + O_2 + e^- \leftrightarrow NaO_2$ (aprotic)	1165	1130	(III) 3.11 (ref. 3) (IV) 2.27 (ref. 4)	(III) 3623 (IV) 2644	(III) 3514 (IV) 5634
Mg	Anode: $Mg + 2OH^- \rightarrow Mg(OH)_2\downarrow + 2e^-$ Cathode: $O_2 + 2H_2O + 4e^- \rightarrow 4OH^-$ Parasitic: $Mg + 2H_2O \rightarrow Mg(OH)_2 + H_2\uparrow$	2205	3836	3.1 (ref. 5)	6836	11892
Zn	Anode: $Zn + 4OH^- \leftrightarrow Zn(OH)_4^{2-} + 2e^-$ $Zn(OH)_4^{2-} \rightarrow ZnO + H_2O + 2OH^-$ Cathode: $O_2 + 2H_2O + 4e^- \leftrightarrow 4OH^-$ Parasitic: $Zn + 2H_2O \rightarrow Zn(OH)_2 + H_2\uparrow$	820	5854	1.65 (ref. 1)	1353	9659
Fe	Anode: $Fe + 2OH^- \leftrightarrow Fe(OH)_2\downarrow + 2e^-$ Cathode: $O_2 + 2H_2O + 4e^- \leftrightarrow 4OH^-$ Parasitic: $Fe + 2H_2O \rightarrow Fe(OH)_2 + H_2\uparrow$	960	7553	1.19 (ref. 6)	1142	8988
Al	Anode: $Al + 4OH^- \rightarrow Al(OH)_4^- + 3e^-$ Cathode: $O_2 + 2H_2O + 4e^- \rightarrow 4OH^-$ Parasitic: $Al + 3H_2O + OH^- \rightarrow Al(OH)_4^- + \frac{3}{2}H_2\uparrow$	2980	8046	2.7 (ref. 7)	8046	21724
Si	Anode: $Si + 4OH^- \rightarrow Si(OH)_4 + 4e^-$ Cathode: $O_2 + 2H_2O + 4e^- \rightarrow 4OH^-$ Parasitic: $Si + 2OH^- + 2H_2O \rightarrow SiO_2(OH)_2^{2-} + 2H_2\uparrow$	3817	8890	2.19 (ref. 8)	8359	19469

* Faraday constant = 26.801 Ah mol^{-1}; Theoretical gravimetric capacity = Faraday constant × atomic weight × number of valence electrons; Theoretical volumetric capacity = theoretical gravimetric capacity × metal density; Gravimetric energy density =

theoretical cell voltage × theoretical gravimetric capacity; Volumetric energy density = theoretical cell voltage × theoretical volumetric capacity.

[§] Based on metal anode alone.

[†] Rechargeable reactions are denoted with "↔" and primary discharge reactions are denoted with "→".

2. Real cell

Photos of the real DEAAC are shown in Fig. 1S. The anode fixture was made of two pieces of PMMA plates with a window of 3 × 4 cm^2 prepared with a laser cutting machine. The PMMA plates were covered with a strong double-adhesive tape (3M™ 468MP Laminating Adhesive, USA) so that the aluminum foil can be glued on it. A piece of aluminum foil was sandwiched between the two PMMA plates with only an area of 3 × 4 cm^2 exposed for reaction. The cell was properly sealed using PARAFILM®. The AAC was set up in a similar fashion using the same cell except that the polymer membrane is removed.

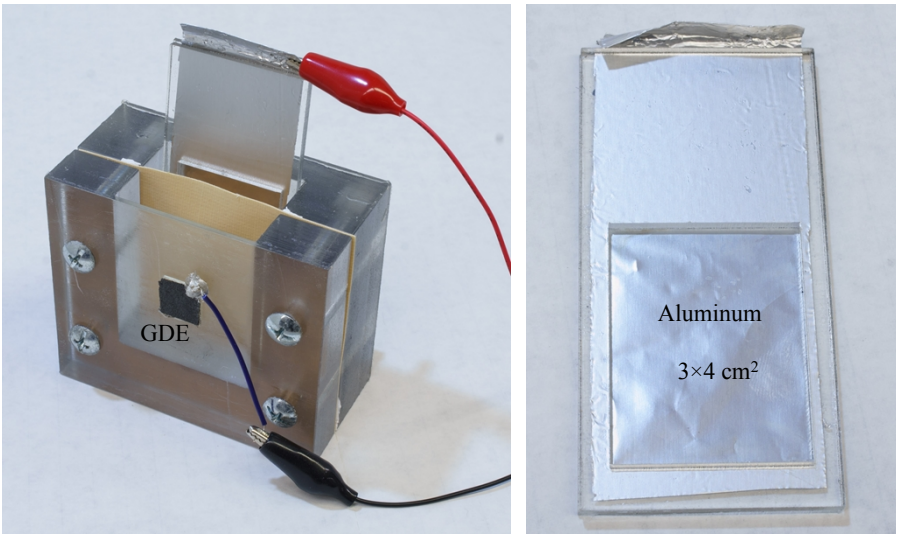

Fig. S1 Photos of the real cell and anode fixture. **(a)** Real DEAAC. **(b)** Anode fixture with an aluminum window of 3 × 4 cm^2.

3. Discharge curve of the AAC at 100 mA cm^{-2}

The discharge curve of AAC at 100 mA cm^{-2} is shown in Fig. S2. The AAC exhibits a flat voltage plateau of ~0.85 V and has a volumetric capacity of ~1700 mAh cm^{-3} and a gravimetric capacity of 630 mAh g^{-1}, which are higher than those at lower discharge current densities. The corresponding volumetric and gravimetric capacities are 1445 Wh L^{-1} and 540 Wh kg^{-1}, respectively.

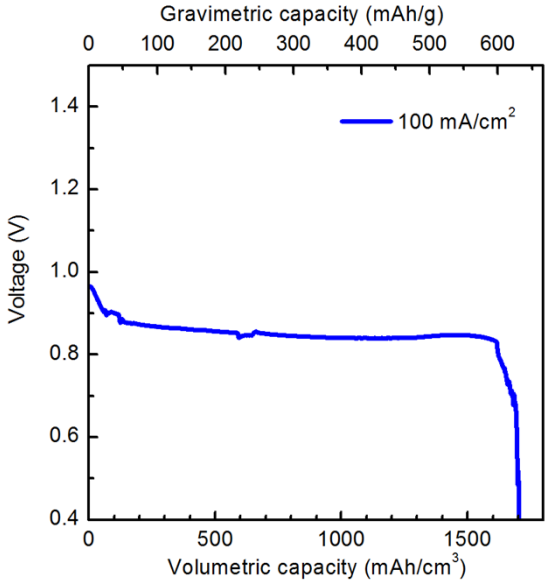

Figure S2. Discharge curve of the traditional AAC at 100 mA cm^{-2}.

4. Detailed calculations for Table 1 in the manuscript

4.1 The Zn/air cell reported by Li *et al.*[9]

The Zn/air primary cell consists of a cathode of CoO/N-CNT loaded carbon paper (1cm^2; catalyst loading of 1mg cm^{-2}), a Zn foil anode and a 6 M KOH aqueous electrolyte of 30−40 mL. Pure oxygen was continuously supplied to the cathode instead of passive airflow. Typical discharge curves were measured under continuous galvanostatic discharge until complete consumption of Zn. The gravimetric capacity was normalized to the mass of consumed Zn. At 10 mA cm^{-2}, the cell exhibited a stable voltage of ~1.3 V with a reported capacity of ~570 mAh g^{-1}. Based on the aforementioned information and the density of zinc (7.14 g cm^{-3}), we can get the volumetric capacity of 4070 mAh cm^{-3} (= 570 mAh g^{-1} × 7.14 g cm^{-3}), the gravimetric energy density of 741 Wh g^{-1} (= 570 mAh g^{-1} × 1.3 V), and the volumetric energy density of 5291 Wh L^{-1} (= 4070 mAh cm^{-3} × 1.3 V).

4.2 The Si/air cell reported by Zhong *et al.*[8]

The Si/air primary cell consists of a nanostructured silicon anode, an air diffusion cathode, and an aqueous KOH electrolyte. It is believed that the nanowire structure greatly increased the Si surface area so not to suffer from passivation as in unmodified Si wafers. The gravimetric capacities of the cell with various KOH concentrations are shown in Table S2 based on the weight of consumed silicon.

Table S2. Gravimetric capacities of the Si/air cell[8]

Discharge current density (mA cm^{-2})	KOH concentration (M)	Weight of consumed silicon (mg)	Gravimetric capacity (mAh g^{-1})
0.05	6	2.26	154.8
0.05	2	1.63	214.7
0.05	0.6	0.49	715.7
0.1	0.6	0.58	1206.0

We picked the setup with the maximum capacity (1206.0 mAh g^{-1}) in Table S2 for comparing with the results of DEAAC. From their reported galvanostatic discharge curves, the corresponding voltage was ~0.85 V. Therefore, together with the density of Si (2.329 g cm^{-3}), we can obtain a volumetric capacity of 2809 mAh cm^{-3} (= 1206 mAh g^{-1} × 2.329 g cm^{-3}), a gravimetric energy density of 1025 Wh kg^{-1} (= 1206 mAh g^{-1} × 0.85 V), and a volumetric energy density of 2387 Wh L^{-1} (= 2809 mAh cm^{-3} × 0.85 V) for this setup.

4.3 The Li/air cell reported by Jung *et al.*[10]

The cell consists of an anode of metallic lithium foil (400 μm thick; maybe excess for the cell anode reaction in order to fully utilize the cathode materials). From their paper, we can obtain the followings:

(1) Li/O_2 cell specifications (CR2032): diameter of 2 cm, height of 3.2 mm and area of 3.14 cm^2.

(2) Discharge specifications: voltage of 2.7 V, current of 500 mA g^{-1}_{carbon} and capacity of 5000 mAh g^{-1}_{carbon}.

(3) Carbon loading density: 1.0±0.1 mg_{carbon} cm^{-2}.

Based on the above information, we can get the volume of Li = 3.14 cm^2 × 400 μm = 0.1256 cm^3, the weight of Li = 0.1256 cm^3 × 0.534 g cm^{-3} = 0.0670704 g, the weight of carbon = 3.14 cm^2 × 1.0 mg_{carbon} cm^{-2} = 3.14 mg. We can further obtain current density = 500 mA g^{-1}_{carbon} × 3.14 mg ÷ 3.14 cm^2 = 0.5 mA cm^{-2} and gravimetric capacity = 5000 mAh g^{-1}_{carbon} × 3.14 mg ÷ 0.0670704 g = 234 mAh g^{-1}_{Li}. Finally, volumetric capacity = 234 mAh g^{-1} × 0.534 g cm^{-3} = 125 mAh cm^{-3}, gravimetric energy density = 234 mAh g^{-1} × 2.7 V = 631.8 Wh kg^{-1} and volumetric energy density = 125 mAh cm^{-3} × 2.7 V = 337 Wh L^{-1}.

4.4 The Na/air cell reported by Hayashi *et al.*[3]

The Na/air primary cell has a structure: Na | Na^+(PC) || Na^+(NASICON) || $Na^+(aq),OH^-(aq),H_2O(l)$ | $O_2(g)$ | Pt. The effective areas of the Na anode, NASICON ceramic membrane, and cathode are 0.36 cm^2, 0.79 cm^2, and 1 cm^2, respectively. The full reaction is

$$Na(s) + \frac{1}{2}H_2O(l) + \frac{1}{4}O_2(g) \rightarrow NaOH(aq)$$

and the anodic and cathodic half reactions are shown in Table 1S. The cell has a V_{OC} of ~2.85 V and a maximum power density of ~5 mW cm^{-2}. The Na/air cell exhibits a capacity of 600 mAh g^{-1} that they calculated based on the total weight of reactants (Na and H_2O) at a discharge current density of 0.63 mA cm^{-2} (normalized by the effective area of the ceramic membrane), and a voltage of ~2.5 V. Based on the stoichiometric ratio of $1:\frac{1}{2}$ for Na:H_2O, we can calculate an equivalent capacity of 835 mAh g^{-1}

$\left(=\frac{23}{23+0.5\times 18}\times 600\ mAh\ g^{-1}\right)$ based on the weight of Na alone. Then the corresponding volumetric capacity is 808 mAh cm^{-3} (= 835 mAh g^{-1} × 0.968 $g{\cdot}cm^{-3}$). Finally, the gravimetric and volumetric energy densities are 2087 Wh kg^{-1} (= 835 mAh g^{-1} × 2.5 V) and 2020 Wh L^{-1} (= 808 mAh cm^{-3} × 2.5 V), respectively. It should be noted that the Na/air cell was tested at a higher temperature of 50ºC with pure O_2. In contrast, our cells were measured at room temperature with passive atmospheric air.

5. Self-corrosion mechanism of aluminum in methanol and aqueous alkaline electrolytes

To study the self-corrosion mechanism of aluminum in methanol and aqueous alkaline electrolytes, a high purity aluminum (99.9991%) was investigated. The specimens were polished using fine sandpapers (P2400 and P4000) with a polishing machine and then were rinsed by DIO water and subsequently acetone. Dimensions and mass of each specimen were measured before corrosion. Three specimens were immersed into a 60 mL 3 M KOH/CH_3OH solution and another three samples into 60 mL 3 M KOH/H_2O. The corrosion for the former was carried out for 40 hours and then the three specimens were rinsed using pure methanol and quickly dried with high-pressure nitrogen. The corrosion for the latter was done for 4 hours and the specimens were rinsed with DIO water instead. Specimens before and after corrosion were weighed and studied with SEM and EDX.

The self-corrosion current density was calculated based on the mass difference before and after corrosion (i.e., mass loss) using the following formula:

$$J_{corr} = \frac{corrosion\ current}{Al\ corrosion\ area} = \frac{charges\ transfered\ in\ corrosion\ \div\ ti}{Al\ corrosion\ area} = \frac{Al\ mass\ loss\ \div\ 27g/mol\ \times\ 3\ \times\ 96485\ C/mol}{Al\ corrosion\ area\ \times\ time}$$

The above formula can also be used to calculate the hydrogen evolution rate because during self-corrosion the valence electrons in aluminum are transferred to form hydrogen through reducing H_2O in the aqueous solution or CH_3OH in the methanol solution, as indicated below:[11]

Self-corrosion in aqueous alkali: $$Al + 3H_2O + OH^- \rightarrow Al(OH)_4^- + \frac{3}{2}H_2\uparrow$$

Self-corrosion in methanol alkali: $$Al + 3CH_3OH + 4OH^- \rightarrow Al(OH)_4^- + 3CH_3O^- + \frac{3}{2}H_2\uparrow$$

The average self-corrosion rate of aluminum in organic electrolyte was calculated to be 1.1164 mA cm^{-2} and that in aqueous electrolyte was 44.4042 mA cm^{-2}. The self-corrosion rate in the methanol solution is only ~2.5% of that in the aqueous solution. This directly explains why aluminum exhibits much higher capacities and energy densities in the DEEAC than in the traditional AAC.

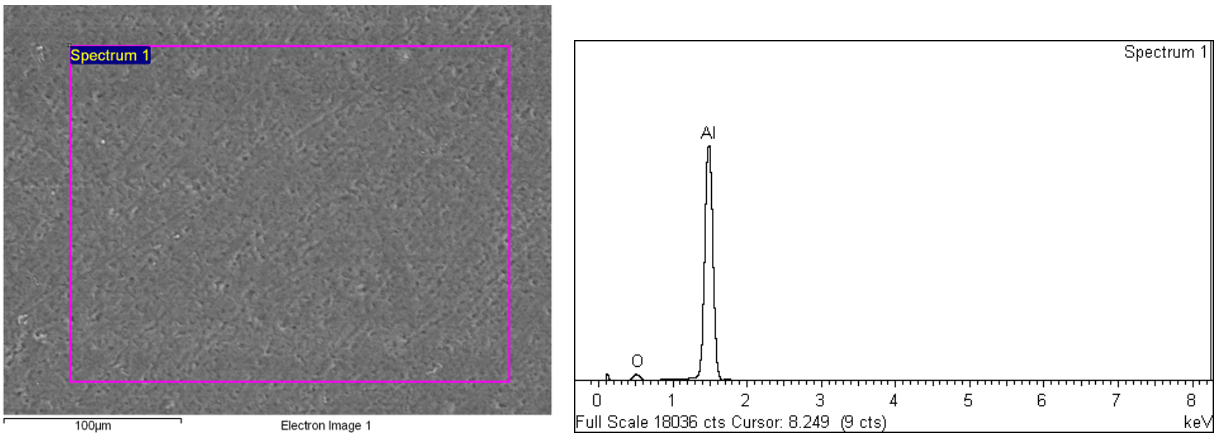

Fig S3. Characterization of an aluminum specimen before self-corrosion. **(a)** SEM image of the specimen surface after polishing with fine sandpaper. **(b)** EDX spectrum showing the composition of the aluminum specimen.

As can be seen from Fig. S3a, the polished specimen has a smooth surface before corrosion. However, the roughness of the aluminum surface dramatically increased after corrosion (Fig S4). For both cases in organic and aqueous solutions, sphere-like features show up on the surface; it is speculated that the self-corrosion prefers to take place along grain boundaries. A thin layer of white powder on the aluminum surface was observed with bare eyes after self-corrosion. We think that this is related to the residual of the reaction product $Al(OH)_3$ that was yet to dissolve

into the strong alkali to form soluble $Al(OH)_4^-$. The similar surface morphology shown in Figs. S4a and S4b also indicates the similar corrosion mechanism in both methanol and aqueous solutions, which is consistent with the findings by Shao *et al.*[12] and Wang *et al.*[11] However, the surface roughness of the specimens in methanol alkaline solutions is less than that in aqueous ones, indicating a more moderate corrosion in the methanol solutions. This is further confirmed with our observation that very few hydrogen bubbles were generated in the organic alkali while the hydrogen generation was violent in the aqueous counterpart. Wang *et al.*[11] found the discharged product on the aluminum surface was mainly a layer of $Al(OH)_3$ for both cases in methanol and aqueous solutions. As far as the chemical composition is concerned, the EDX spectra of specimens before- and after-corrosion look similar, showing mainly the component of aluminum (Fig. S3b); the layer of $Al(OH)_3$ is too thin to be detected with EDX.

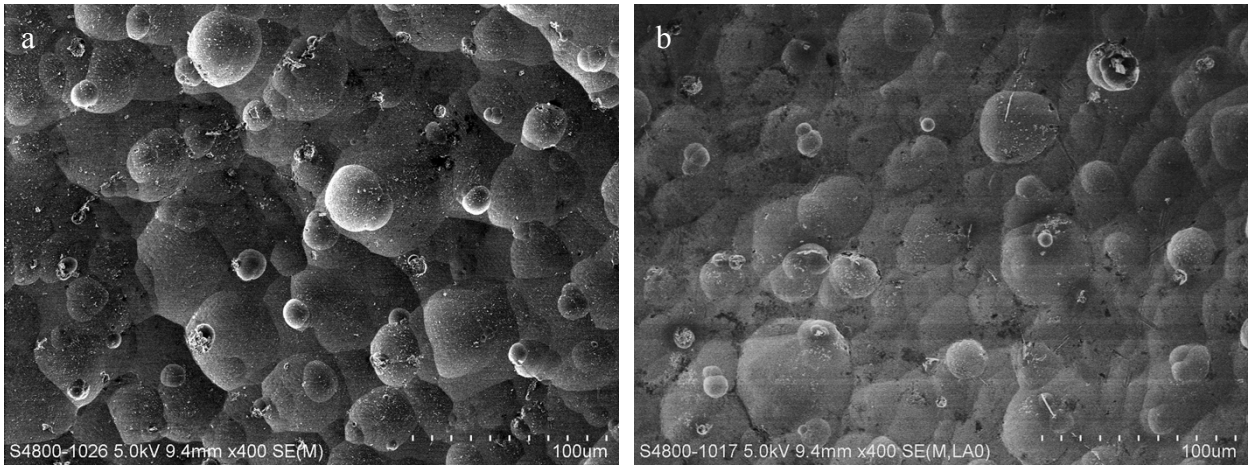

Fig S4. Characterization of two aluminum surfaces after self-corrosion. **(a)** SEM image of an aluminum specimen after corrosion in the aqueous solution. **(b)** SEM image of an aluminum specimen after corrosion in the organic solution.

References

1. J. S. Lee, S. T. Kim, R. Cao, N. S. Choi, M. Liu, K. T. Lee and J. Cho, *Adv Energy Mater*, 2011, **1**, 34−50.
2. Y. Y. Shao, F. Ding, J. Xiao, J. Zhang, W. Xu, S. Park, J. G. Zhang, Y. Wang and J. Liu, *Adv Funct Mater*, 2013, **23**, 987−1004.
3. K. Hayashi, K. Shima and F. Sugiyama, *J Electrochem Soc*, 2013, **160**, A1467−A1472.
4. P. Hartmann, C. L. Bender, M. Vracar, A. K. Durr, A. Garsuch, J. Janek and P. Adelhelm, *Nat Mater*, 2013, **12**, 228−232.
5. W. Y. Li, C. S. Li, C. Y. Zhou, H. Ma and J. Chen, *Angew Chem Int Edit*, 2006, **45**, 6009−6012.
6. B. T. Hang, T. Watanabe, M. Egashira, I. Watanabe, O. Shigeto and J. Yamaki, *J Power Sources*, 2006, **155**, 461−469.
7. D. R. Egan, C. Ponce de León, R. J. K. Wood, R. L. Jones, K. R. Stokes and F. C. Walsh, *J Power Sources*, 2013, **236**, 293−310.
8. X. Zhong, H. Zhang, Y. Liu, J. W. Bai, L. Liao, Y. Huang and X. F. Duan, *Chemsuschem*, 2012, **5**, 177−180.
9. Y. G. Li, M. Gong, Y. Y. Liang, J. Feng, J. E. Kim, H. L. Wang, G. S. Hong, B. Zhang and H. J. Dai, *Nat Commun*, 2013, **4**, 1805.
10. H. G. Jung, J. Hassoun, J. B. Park, Y. K. Sun and B. Scrosati, *Nat Chem*, 2012, **4**, 579−585.
11. J.-B. Wang, J.-M. Wang, H.-B. Shao, J.-Q. Zhang and C.-N. Cao, *Journal of Applied Electrochemistry*, 2007, **37**, 753−758.
12. H. Shao, J. Wang, X. Wang, J. Zhang and C. Cao, *Electrochem Commun*, 2004, **6**, 6−9.